Fall 12-2019

Towards the Synthesis of an Artificial Fluorescent Siderophore

Ashley Burns
University of Southern Mississippi

The University of Southern Mississippi

Towards the Synthesis of an Artificial Fluorescent Siderophore

by

Ashley Burns

A Thesis
Submitted to the Honors College of
The University of Southern Mississippi
in Partial Fulfillment
of Honors Requirements

December 2019

Approved by:

_____
Karl J. Wallace, Ph.D., Thesis Adviser
Associate Professor of Chemistry

_____
Bernd Schroeder, Ph.D., Director
School of Mathematics and Natural Sciences

_____
Ellen Weinauer, Ph.D., Dean
Honors College

Abstract

Siderophores are molecules capable of binding ferric ions with high affinity (K_a = 10^{52}). This thesis outlines our attempts to synthesize an artificial siderophore, which incorporates a signaling group to help monitor the uptake of ferric ions. The artificial siderophore is a tripodal molecular receptor synthesized in a five-step procedure with a proposed final sixth step. Rhodamine 6G azide (95.0% yield) was formed from rhodamine 6G and the synthesis of 2-azidoethanamine was modified from the literature. The tripodal arm portion of the sensor was successfully synthesized by protecting the catechol of 2,3-dihydroxybenzaldehyde to form 3-formyl-1,2-phenylene dimethanesulfonate (98.8% yield). The reduction of the aldehyde in the previous compound to a primary alcohol formed 3-(hydroxymethyl)-1,2-phenylene dimethanesulfonate (86.6% yield), which then underwent a nucleophilic substitution to yield 3-(bromomethyl)-1,2-phenylene dimethanesulfonate (80.0% yield). The product of the nucleophilic substitution then successfully underwent a bimolecular nucleophilic substitution to yield the mesyl protected tripodal arm (76.8% yield).

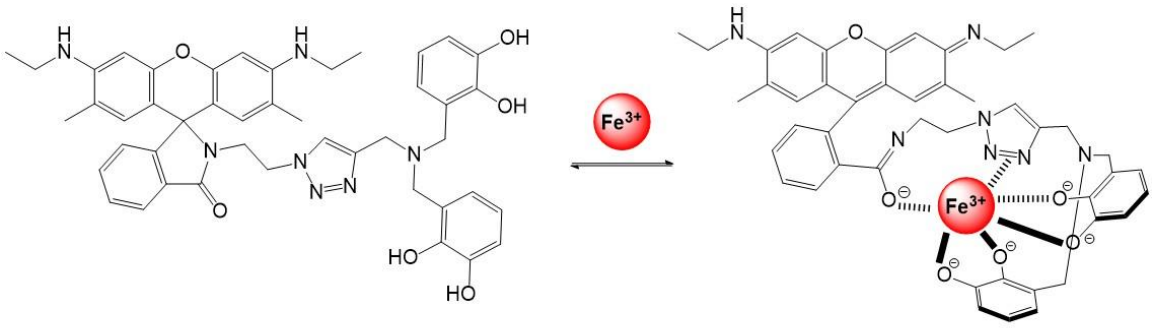

Ring Closed
Non-Fluorescent

Ring Open
Fluorescent

Keywords: siderophore, ferric ions, rhodamine, off-on sensor, spirolactam ring, fluorescence

Acknowledgements

I would like to acknowledge my thesis advisor, Dr. Karl Wallace, for guiding me through this research experience as well as Ashley Johnson for taking the time and effort to teach me the laboratory methods and procedures. Thank you both. To the professors that have educated me over the past three years, I thank you all for the knowledge I have learned and retained.

Additionally, I would like to acknowledge caffeine, as I would not have made it this far without the Starbucks in the Cook Library.

Table of Contents

List of Tables

List of Figures

List of Schemes

List of Abbreviations

CH_3CN	Acetonitrile
$CuSO_4$	Copper(II) sulfate
DCM	Dichloromethane
DMSO	Dimethylsulfoxide
eq	Equivalence
EtOAc	Ethyl acetate
Fe^{3+}	Ferric ion
Fe^{2+}	Ferrous ion
HEPES	4-(2-hydroxyethyl)-1-piperazineethanesulfonic acid)
HSAB	Hard-soft acid-base
IR	Infrared
K_d	Dissociation constant
KOH	Potassium hydroxide
M^0	Free metal ion
m/z	Mass-to-charge ratio
MeOH	Methanol
$MgSO_4$	Magnesium sulfate
MS	Mass spectrometry
MsCl	Mesyl chloride
Na_2SO_4	Sodium sulfate
$NaBH_4$	Sodium borohydride
NaN_3	Sodium azide

$NaNO_3$	Sodium nitrate
NMR	Nuclear magnetic resonance
OH	Hydroxy
PBr_3	Phosphorous tribromide
Ph	Phenyl
py	Pyridine
rt	Room temperature
TBDMS	Tert-butyldimethylsilyl chloride
TEA	Triethylamine
THF	Tetrahydrofuran
Tris-HCl	2-Amino-2-(hydroxymethyl)-1,3-propanediol hydrochloride
xs	Excess

Chapter 1 - Introduction

1.1 General Siderophore and Iron Background

Iron is considered an essential trace element, or an element present in amounts of $mg \cdot kg^{-1}$ or lower, required for biological and metabolic activities.[1–3] Siderophores (Greek for "iron carrier") are molecules with a high affinity for ferric ions (Fe^{3+}) typically produced by bacteria and plants.[4–9]

Ferric ions are known as "hard" acids, and they will form thermodynamically stable bonds with "hard" bases (Table 1.1). The hard and soft nature of a Lewis acid and base can be described as follows: "hard," or nonpolarizable, small ionic radius, highly charged, and resists oxidation; and "soft," or polarizable, large ionic radius, not highly charged, and susceptible to oxidation.[10] The Fe^{3+} ions are classified as hard Lewis acids, which will readily coordinate to hard or borderline Lewis bases, especially those containing oxygen and nitrogen atoms with lone pairs of electrons.

Table 1.1: Lewis acids and bases categorized into hard, borderline, and soft.

	Lewis Acids	Lewis Bases
Hard	$AlCl_3$, BF_3, H^+	H_2O, OH^-, NH_3
	Fe^{3+}, Cr^{3+}, Mg^{2+}	Cl^-, F^-, NO_3^-
Borderline	Fe^{2+}, SO_2, Zn^{2+}	N_3^-, py, $PhNH_2$
Soft	Ag^+, Pt^{2+}, Cd^{2+}	SCN^-, CN^-, SH^-
	BH_4, Au^+, M^0	CO, I^-, $S_2O_3^-$

The proposed sensor design utilizes these acid-base definitions to better understand the coordinating nature of Fe^{3+} ions to Lewis basic sites. With this understanding, the synthesis route for the sensor can focus on the addition of hard Lewis

basic sites exhibiting enhanced coordination to Fe^{3+} ions, thus better mimicking the Lewis basic sites present on natural siderophores.

1.2 Biological Importance of Ferric Iron

Ferric ions are essential in the metabolism of oxygen, regulation of body temperature, and synthesis of ribonucleic acid and deoxyribonucleic acid.[11,12] The concentration of Fe^{3+} ions in biological systems must be monitored to ensure avoidance of excess or deficient Fe^{3+} ion concentrations.[13] Ferric ions in excess, or concentrations lower than the proposed daily dietary allowance of 8 mg for males and 18 mg for females aged 19 to 50 years have been linked to possible causes for the development of neurodegenerative diseases including Parkinson's and Alzheimer's disease (Table 1.2).[14–17] Ferric ion deficiency is measured by analyzing the serum ferritin concentration. When the serum ferritin concentration has dropped to 12 $\mu g \cdot L^{-1}$ or lower, all stores of iron in the body have been depleted.[17] Iron deficiency can lead to heart failure, kidney damage, anemia, and liver damage (Table 1.2).[1,17,18]

Table 1.2: Biological benefits, excess, and/or deficiency in common metal ions.[12,17,19–21]

Metal ion	Biological Functions	In Excess/Deficiency	Upper Intake Levels (mg)
Fe^{2+}/Fe^{3+}	Oxygen uptake, electron transfer, oxygen metabolism	Low oxygen delivery, low blood pressure, anemia	45
Cu^{2+}	Bone formation, development of connective tissues	Wilson's disease, cellular metabolism interference, liver cirrhosis	10
Hg^{2+}	none	Neurotoxin (methylmercury)	0.002 (weekly)

1.3 Environmental Siderophores

Bacteria and plants growing in iron-depleted conditions produce siderophores to aid in iron acquisition. For example, Enterobactin, (Figure 1.1) a common, naturally occurring siderophore, is found in bacteria such as *Escherichia coli*.[2223]

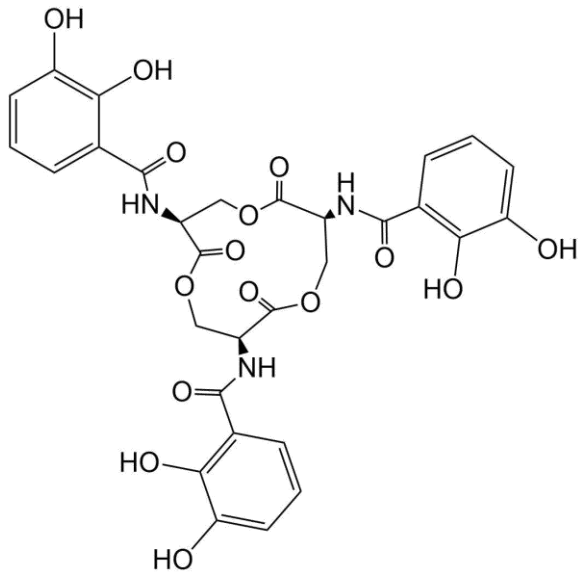

Figure 1.1: Structure of Enterobactin.

Many siderophore-producing bacteria are located in ocean waters where iron is present in less than 1×10^{-6} M, which is lower than optimal for the growth of marine bacteria.[24] To acquire iron for the growth of bacteria, the organisms produce siderophores to increase the concentration of iron in the bacteria's system. For example, Enterobactin binds Fe^{3+} ions in a 1:1 molar ratio with a binding affinity of 10^{52} M^{-1}.[25] However, not all bacteria can produce siderophores but can acquire siderophores produced by other bacteria for iron transport. Bacteria incapable of producing native siderophores may also extracellularly reduce ferric ions to ferrous ions (Fe^{2+}) as a substitute method to increase iron concentration within the bacteria.[25–27]

1.4 Biological Applications of Artificial Siderophores

The industrial push for the synthesis of artificial siderophores that can operate within physiological conditions (pH 7.35-7.45) has increased with the hopes of utilizing the probes for the specific and sensitive detection of metal ions in biological systems.[28] The rhodamine dye has been shown to act as both the chelate motif and a chromophore to bind and monitor metal ions in biological applications, given that the physiological pH resides within the optimal pH range for rhodamine-based probes. Studies concerning the stability of rhodamine-based artificial siderophores used in biological systems are being conducted. The probes have been tested in human breast cancer cells (MCF-7 cells) for cytotoxicity, and have been implanted into Zebrafish embryos.[29–32] In addition, enzymes that process substrates involved in the synthesis of biosynthetic siderophore analogs have been explored for use in biological systems as inhibitors in antibiotic research.[33,34]

1.5 Artificial Siderophore Synthesis in the Wallace Research Group

The synthesis of artificial siderophores has been investigated in order to develop sensitive probes for the detection of a select metal or group of metals. Rhodamine-based compounds have successfully been incorporated into artificial siderophore synthesis strategies to aid monitoring the ferric ions via a colorimetric and fluorescence optical response. These fluorescence and colorimetric responses are easily quantified using absorption and fluorescence bands, typically seen between 500 and 600 nm.[35–37] Colorimetric probes are favorable in metal detection research, as an optical response can be determined by naked-eye detection.[11] This type of sensor is commonly referred to as an “off-on” molecular probe, as the sensor is colorless in the absence of ferric ions, but an optical response is seen upon the addition of ferric ions.

The Wallace Group has prepared molecular probes to monitor different cationic species, for example Cu^{2+}, Fe^{3+}, Fe^{2+}, and Zn^{2+} ions. Based on this previous work we developed a synthetic strategy to prepare sensor **1.0** (Figure 1.2). This strategy builds upon an existing rhodamine molecule in order to optimize the selectivity of previous probes in the detection of Fe^{3+} ions in ultralow concentrations without interference from Cu^{2+}, Fe^{2+}, and Hg^{2+} ions.

Molecular sensor **1.0** was designed based on the structure requirements of natural siderophores to mimic the binding sites proven to coordinate with Fe^{3+} ions. The catechol groups (highlighted red) in the Enterobactin structure will be incorporated into the molecular receptor on compound **1.0** to coordinate with Fe^{3+} ions (Figure 1.2). Therefore, two catechol binding sites and another coordination environment (highlighted blue) will form three bidentate motifs needed to encapsulate the metal ion in a thermodynamic manner, based on the chelate effect and hard-soft acid-base (HSAB) nature of the Lewis acid-base adduct (Figure 1.2). The proposed synthetic route would allow us to design a tripodal molecular sensor, mimicking a biological receptor, anticipated to coordinate iron within the ultralow concentration (1×10^{-9} M to 1×10^{-15}) range.

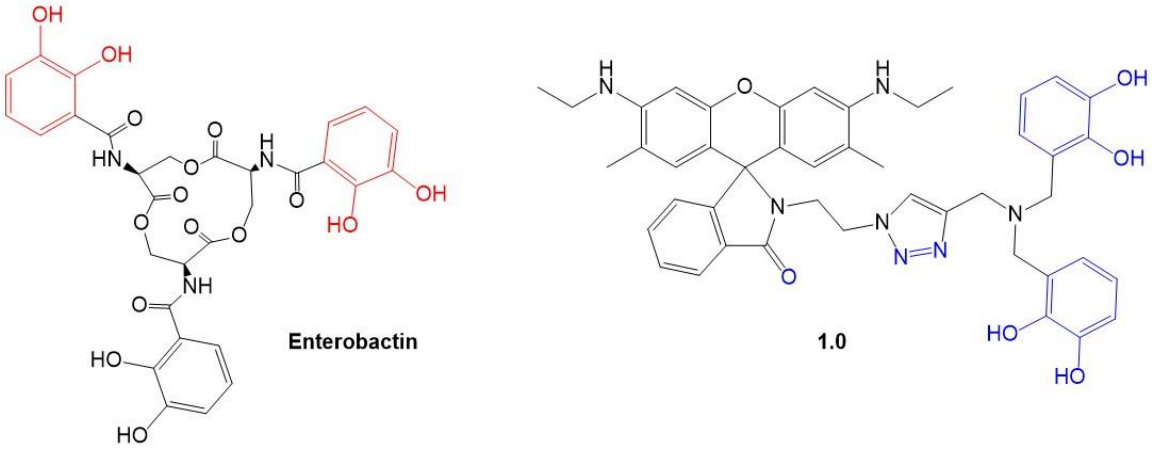

Figure 1.2: Comparison of Enterobactin and proposed sensor. The catechols (red) and binding sites (blue) are shown here.

Chapter 2 - Literature Review

2.1 Artificial Siderophores

Siderophores have been explored for the purpose of transporting Fe^{3+} ions across cell membranes to regions of depleted ferric ion concentration. Artificial siderophores have advantages over naturally occurring molecules (Table 2.1). These advantages include more straightforward synthesis and fine-tuned solubility in varying environments.[38] Artificial siderophores may also be manipulated to increase coordination of metal ions by adding functional groups.[38] Artificial siderophores utilize Lewis bases as functional groups to resemble the general structure and coordinating function of the groups seen on natural siderophores (Table 1.2). When synthesizing an artificial siderophore, the resulting chelate ring size, overall stability, additional functional groups, and hydrophilic or hydrophobic properties should be considered in order to manage the siderophore's sensitivity and selectivity for Fe^{3+} ions.[26]

Table 2.1: Broad advantages and disadvantages of artificial siderophores.

	Advantages	Disadvantages
Artificial Siderophores	Fine-tuned solubility in varying environments; Manipulated to exhibit specific binding environments	Must be synthesized; Trial and error in synthesizing expected binding environments

2.2.0 Rhodamine-based Synthesis Methods for Artificial Siderophores

Rhodamines, a family of fluorescent dyes, have been utilized as a spectroscopic handle to help monitor the analyte. The rhodamine functional group can act as both a chromophore and a fluorophore. Two "classic" rhodamine dyes often used in sensor

design are rhodamine B and rhodamine 6G (Figure 2.1).[39] Derivatives of rhodamine have been extensively utilized due to their desired properties, such as water solubility and stability (thermal and light). These properties can be desirable in an artificial probe that is frequently exposed to natural light.[40,41] Bioavailability properties may also be increased when using rhodamine. Longer emission (>590 nm) and excitation (>550 nm) wavelengths and larger coefficients of absorption can also be observed with rhodamine dyes.[37,42]

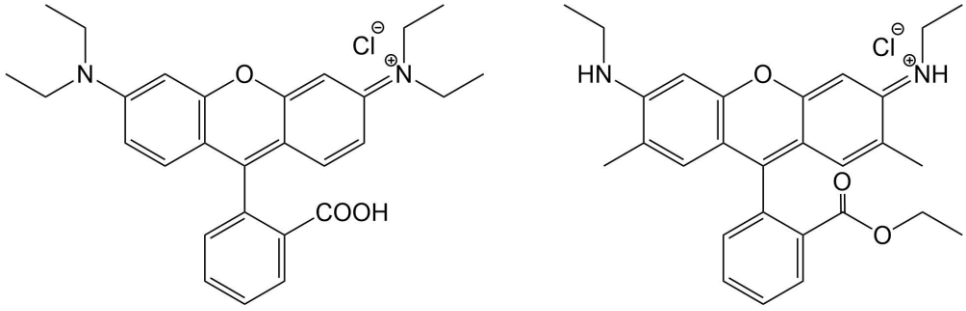

Figure 2.1: Two common rhodamine molecules used in probe synthesis.

The sensing mechanism of rhodamines, namely the spirolactam ring opening and closing, allows for the dye's simple "off-on" sensing. When a rhodamine molecule forms a chelating complex with a metal cation, such as the Fe^{3+} ion, a spirolactam ring opening occurs (Scheme 2.1).[43] The spirolactam, when closed, exhibits sp^3 hybridization and is considered to be in the "off" position. When the ring-opening occurs, the hybridization of the carbon atom (highlighted red) changes from sp^3 to sp^2 hybridization, and a spectroscopic signal is seen, i.e., turns "on." Upon ring-opening of the spirolactam ring, the molecule exhibits a characteristic absorbance band near 560 nm and a fluorescence band near 600 nm as the color of the solution changes from colorless to pink.[44–46] The color change acts as a "switch," determining when the complex with the probe has either

formed or disappeared.[47–49] This change can be detected by our eye as a distinct color change is observed. A significant drawback is the lack of sensitivity in colorimetric systems.[50] However, another optical feature of these molecules is that these compounds are fluorescent. The fluorescent properties of rhodamine dyes have aided in the molecules' extensive use in detectors for metal ions.[47,48]

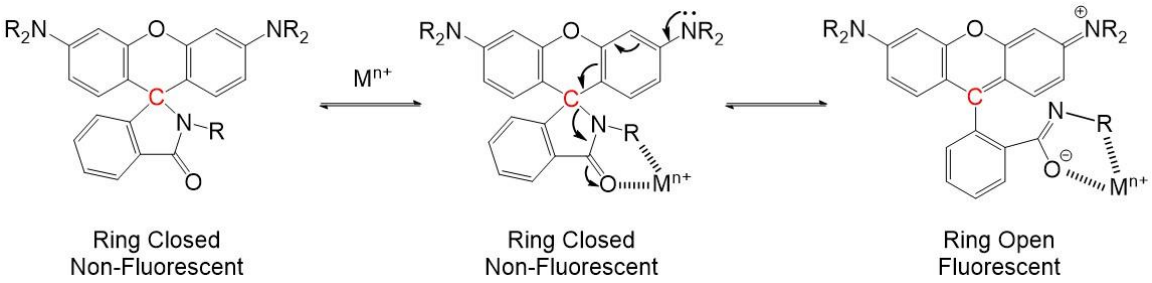

Scheme 2.1: Spirolactam ring-opening in response to metal ion coordination produces an "on" response. The coordinating ion, M^{n+}, indicates a nonspecific metal ion capable of binding to the sensor.[44]

When synthesizing a rhodamine-based sensor, the coordination environment of the final molecular probe must be considered to accurately predict metal ion binding. In general, Fe^{3+} ions will bind to several common motifs (Table 2.2).

Table 2.2: Common ligands capable of binding to Fe^{3+} ions.

Monodentate	Bidentate	Hexadentate
Cl^- H_2O CN^-	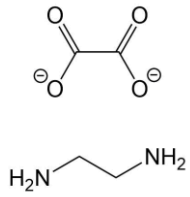	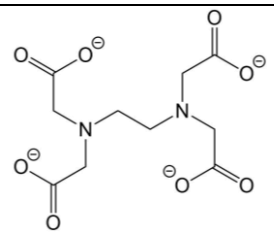

2.2.1 Rhodamine B Derived Molecular Probes for Fe^{3+} Ions

Rhodamine B is one of the rhodamine dyes frequently used for the selective detection of Fe^{3+} ions.[15,31,42] Yang et al.[35] utilized rhodamine B to synthesize a probe with increased selectivity for Fe^{3+} ions over other trivalent metal ions in bioimaging

applications. The proposed mechanism for Yang et al.'s probe **2.1** involved a spirolactam ring opening (Scheme 2.2).

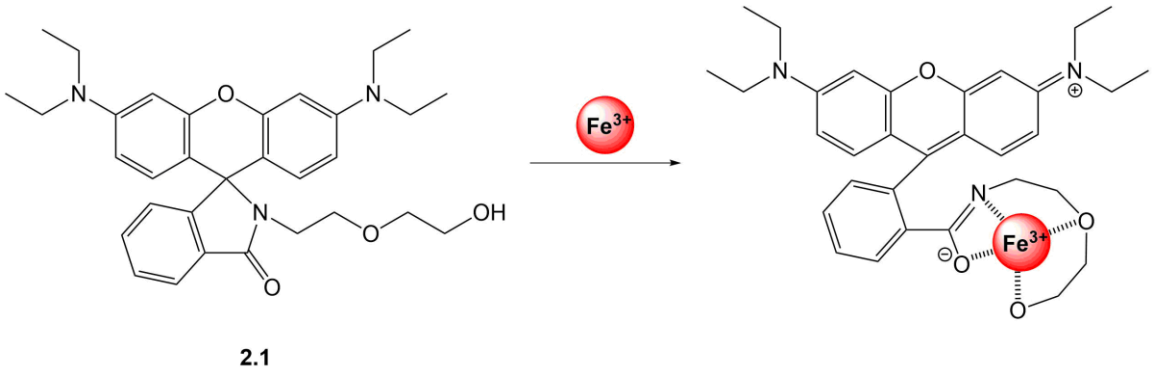

2.1

*Scheme 2.2: Ring-opening of probe **2.1** for selective Fe^{3+} ion detection.*[35]

The response of probe **2.1** in various pH buffers was studied to determine the pH range in which the probe exhibited the lowest absorbance. The optimal pH range was shown to be between 4 and 10. Below pH 4, the spirolactam ring, which exhibits proton-driven ring openings, was affected by the acidic solution. Since physiological pH resides between 7.35 and 7.45 in blood and plasma, probe **2.1** was determined unaffected and, thus, useful for possible Fe^{3+} ion detection at physiological pH.[28]

In addition, Yang et al.[35] performed titrations in a Tris-HCl buffered solution (pH 7.3) in a water-DMSO mix (99:1, v/v) to determine the response of probe **2.1** to an increasing concentration of Fe^{3+} ions.[35] A constant concentration of probe **2.1** was maintained as the concentration of Fe^{3+} increased. The results indicated an increased fluorescence intensity at 585 nm and an absorption peak at 561 nm.[35] The increased absorption band could be easily observed as the probe-ion coordination complexes formed and turned the solution from clear to pink. The maximum absorbance recorded occurred when ion concentration versus ion-probe concentration was 0.5, indicating the probe formed a 1:1 complex with the ions present.[35] Drastic hyperchromic shifts in the

fluorescence intensity spectra or absorption spectra did not occur when the probe was introduced to monovalent and divalent metal ions. A slight hyperchromic shift at 560 nm was reported when probe **2.1** was in contact with Al^{3+} and Cr^{3+} ions, but the increase in fluorescence intensity was not nearly as large as the increase in intensity occurring from contact with Fe^{3+} ions (Figure 2.2).[35]

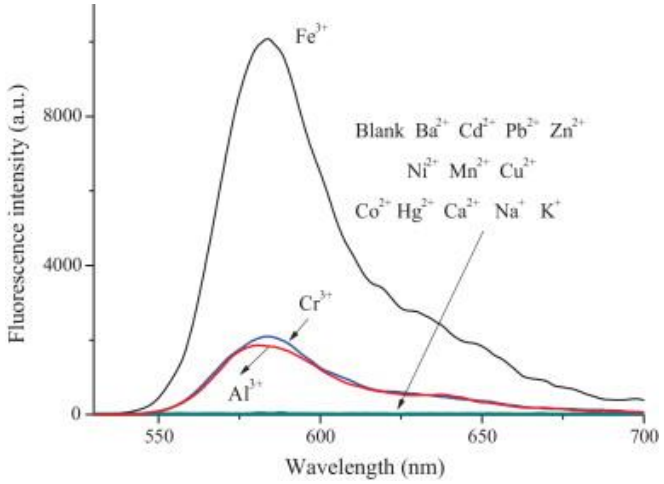

*Figure 2.2: Hyperchromic shifts of metal ions introduced to probe **2.1** in solution. Reprinted from Chin. Chem. Lett., 26, Yang et al., A Simple, Water-soluble, Fe^{3+}-selective Fluorescent Probe, 129-132, Copyright (2015), with permission from Elsevier.*

In a similar study, Nayab et al. synthesized probe **2.2** from rhodamine B hydrazide for Fe^{3+} ion detection. [36] The proposed mechanism for probe **2.2** involved a similar spirolactam ring opening to form an intermediate, which is then hydrolyzed to rhodamine B to resolve the intermediate's instability (Scheme 2.3). Nayab et al. based this mechanism on mass spectrometry (MS) data. [36] Before the addition of Fe^{3+}, the mass-to-charge ratio for probe **2.2** was *m/z* = 587. With the addition of Fe^{3+}, the prominent mass-to-charge ratios were *m/z* = 443 and *m/z* = 471, indicating the original probe fragmented to yield the intermediate compound (*m/z* = 471).[36]

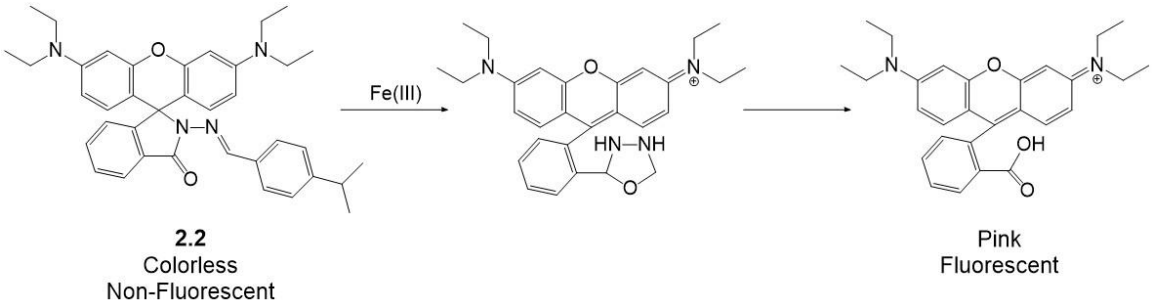

*Scheme 2.3: Proposed coordination of probe **2.2** for Fe^{3+} ions. The structure in the middle is unstable and hydrolyzed to yield the product on the right.*[36]

Probe **2.2** was found to exhibit its lowest pH-dependent absorbance within a pH range from 5 to 8, which indicated the optimal use of the probe in physiological pH similar to Yang et al.'s[35] probe **2.1**.[36] Probe **2.2** was introduced to aqueous solutions containing different metal ions in acetonitrile (CH_3CN)-aqueous HEPES buffer (5:5, v/v; pH 7.2) and resulting fluorescence intensity or absorbance bands were recorded (Figures 2.3(a) and 2.3(b)). Probe **2.2** exhibited hyperchromic shifts in fluorescence intensity at 585 nm and absorbance at 550 nm when in contact with Fe^{3+} ions. A color change from clear to pink served as a naked-eye detection for the hyperchromic shift in absorption. Probe **2.2** did not exhibit hyperchromic activity when in contact with the other added metal ions, thus reinforcing the ability of the probe to selectively interact with Fe^{3+} ions in solution. Additionally, the detection limit of probe **2.2** was calculated to be 5.1×10^{-6} M, the association constant was determined to be 3.4×10^{4} M^{-1}, and the molar fraction of $[Fe^{3+}]/[Fe^{3+}]$[probe **2.2**] indicated a 1:1 complex formation.[36]

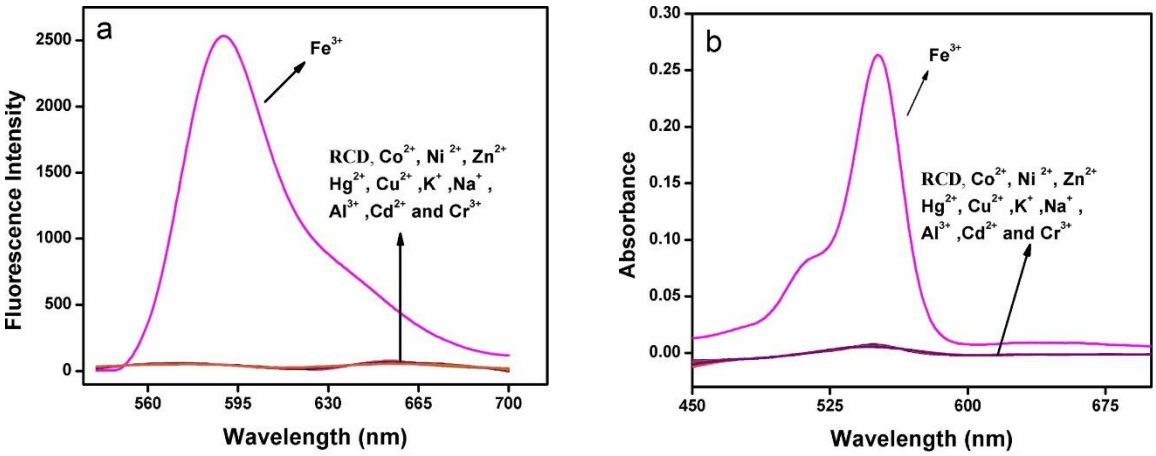

*Figure 2.3: (a) Fluorescence and (b) absorbance spectra resulting from probe **2.2**-ion complex. Reprinted from J. Photochem. Photobiol., 347, Nayab et al., A Highly Sensitive "Off-On" Optical and Fluorescent Chemodosimeter, 209-217, Copyright (2017), with permission from Elsevier.*

Similarly, Sheng et al. synthesized a selective rhodamine B-based probe, probe **2.3**, for the detection of Fe^{3+} ions over Cr^{3+} ions.[51] Absorption studies and fluorescent titrations were performed in a methanol/water (1:99) buffered solution (20 mM HEPES, 50 mM $NaNO_3$, pH 7.0).

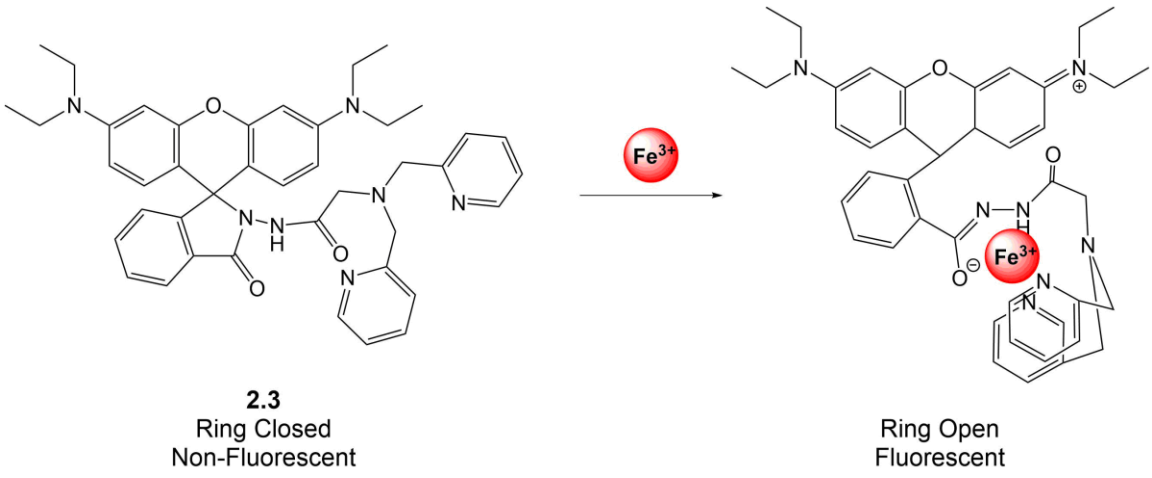

*Scheme 2.4: Ring opening for probe **2.3** coordination to Fe^{3+} ions.*[51]

When probe **2.3** was introduced to Fe^{3+} ions in solution, the complex formed and exhibited a bright red color indicated by the increase in the absorption spectra of the solution near 568 nm. Prior to the addition of Fe^{3+} ions, the absorption spectra of probe **2.3** lacked absorption in the 500 nm region, and the spirolactam ring remained closed

(Scheme 2.4). When both Fe^{3+} ions and Cr^{3+} ions were introduced to probe **2.3**, the resulting fluorescence intensity recorded a notable hyperchromic shift, indicating that the spirolactam ring had opened. No color change occurred when in contact with Cr^{3+} ions, indicating that the probe **2.3** exhibited a greater selectivity for Fe^{3+} ions over other +3 charged metal ions.[51] Additionally, the molar fraction of $[Fe^{3+}]/[Fe^{3+}]$[probe **2.3**] indicated formation of a 1:1 complex when probe **2.3** was introduced to Fe^{3+} ions in solution, and the K_d was determined to be 1.9×10^{-5} M.[51]

2.2.2 Rhodamine 6G for the Detection of Fe^{3+} Ions

Rhodamine 6G has also been incorporated into molecular probes. Kim et al.[37] chose rhodamine 6G in the synthesis of probe **2.4** immobilized in silica. Advantages of immobilizing the probe in silica over other explored trivalent metal ion-detecting probes included higher porosity, increased surface area, and greater thermal stability. The synthesis of the immobilized probe seemed superior to conventional probe synthesis given the resulting compact probe design and decrease in the volume of fluid consumption.

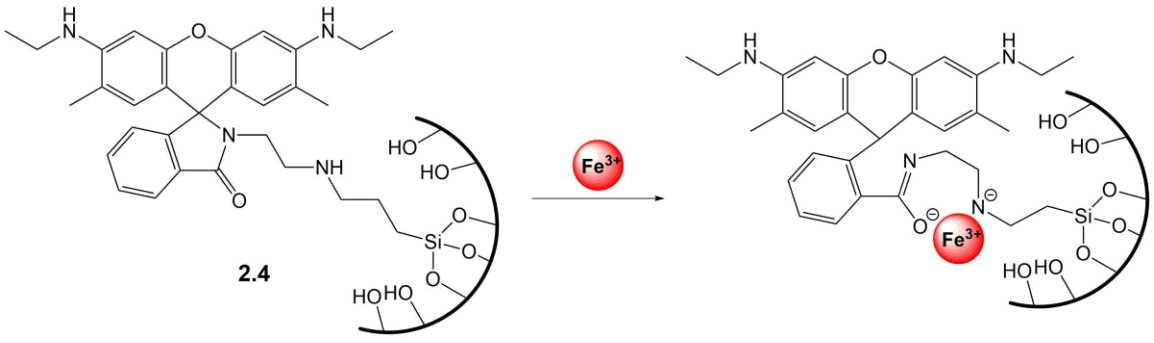

*Scheme 2.5: Proposed coordination of silica-immobilized probe **2.4** to Fe^{3+} ions.*[37]

Absorption studies and fluorescent titrations were performed in aqueous solution. To indicate the selectivity of probe **2.4** towards Fe^{3+} ions over other metal ions, various metal ions were introduced to the probe solution. The most prominent fluorescence intensity of probe **2.4** was exhibited at 552 nm when in contact with Fe^{3+} ions, which promoted ring-opening (Scheme 2.5). This probe-ion complex exhibited a fluorescent yellow hue (Figure 2.4). Probe **2.4** was shown to be less selective for Fe^{3+} ions than probe **2.2**[36] as probe **2.4** formed complexes with Al^{3+} and Hg^{2+} to generate hyperchromic shifts in fluorescence intensity at 552 nm. However, due to the large gap in intensity between the Fe^{3+} ion band and Al^{3+} and Hg^{2+} bands, probe **2.4**'s selectivity for Al^{3+} and Hg^{2+} ions was deemed negligible as no shifts in emission were recorded.[37] Additionally, the association constant for Fe^{3+} ions was calculated to be 8.5×10^3 M^{-1}.[37]

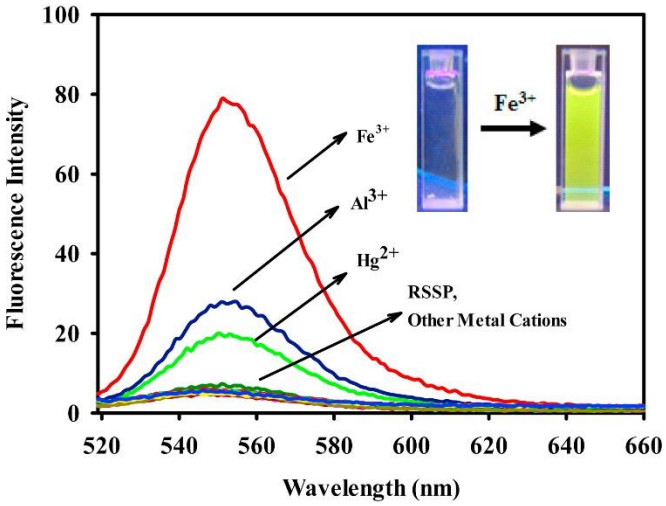

*Figure 2.4: Hyperchromic shifts in fluorescence intensity observed when probe **2.4**-ion complex formed. Reprinted from Sens. Actuators, B, 224, Kim et al., A Rhodamine Scaffold Immobilized onto Mesoporous Silica, 404-412, Copyright (2016), with permission from Elsevier.*

2.3 Improvements in Selectivity and Sensitivity

After reviewing previous advancements in rhodamine-based sensors for the detection of Fe^{3+} ions, one may conclude that most sensors are sensitive to Fe^{3+} ions but not entirely selective. In some cases, such as the rhodamine 6G based probe synthesized

by Kim et al.[37], the probe forms complexes with other metal ions that are, however, characterized by minimal hyperchromic shifts in fluorescence intensity. The sensor synthesized in this research project looks to increase the selectivity of the rhodamine-based sensor for Fe^{3+} ions to yield a selective Fe^{3+} ion molecular probe.

Chapter 3 - Materials and Methods

3.1 General Techniques

One-dimensional (^{1}H, ^{13}C) NMR spectra were recorded on a Bruker Ultrashield plus 400 MHz spectrometer in the appropriate deuterated solvents or on a Bruker Advance 600 MHz spectrometer. Chemical shifts are reported in parts per million (ppm) downfield from tetramethylsilane (0 ppm) as the internal standard and coupling constants (*J*) are recorded in hertz (Hz). The multiplicities in the ^{1}H NMR spectra are reported as (br) broad, (s) singlet, (d) doublet, (dd) doublet of doublets, (ddd) doublet of doublet of doublets, (t) triplet, (sp) septet and (m) multiplet. All spectra are recorded at ambient temperature. UV-Vis spectra were recorded on a Beckman DU-70 UV-Vis spectrometer. Low-resolution mass spectra were measured with Finnigan TSQ70 and VG Analytical ZAB2-E instruments. IR spectra were recorded on a Nicolet Nexus 470 FT-IR paired with a Smart Orbit ATR attachment; the characteristic functional groups are reported in wavenumbers (cm^{-1}), and are described as weak (w), medium (m), strong (s) and very strong (vs).

3.2 Experimental Procedures

Rhodamine 6G azide (3.4)

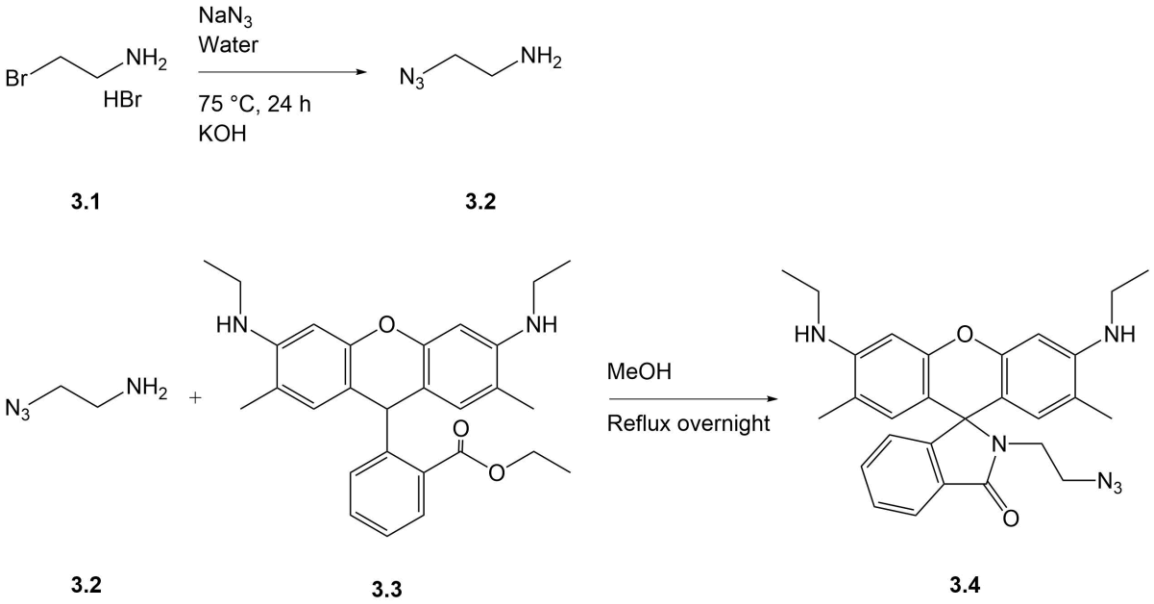

The experimental procedure for the sysnthesis of compound **3.2** was modified from literature.[52] Sodium azide (1.77 g, 0.026 mol) and 2-bromoethylamine hydrobromide (1.77 g, 0.009 mol) were added to water (5.0 mL) and heated and stirred for 24 h at 75 °C. The reaction was cooled to 0 °C. Aqueous potassium hydroxide was added to adjust the pH to 9. The solution was extracted with ether. The resulting organic layer was washed with saturated sodium chloride solution and dried using sodium sulfate (Na_2SO_4). The Na_2SO_4 was filtered out of the solution, and excess solvent was removed from the filtrate under reduced pressure. The desired product, compound **3.2**, was a yellow oil. The yield of compound **3.2** was not calculated to reduce product loss due to the extreme volatility and the amount required for the next step in the reaction. ^{1}H NMR (400 MHz, $CDCl_3$): δ, ppm 3.35 (1H, t, *J* = 5.6 Hz), 2.86 (2H, t, *J* = 5.6 Hz), 1.52 (2H, s). ^{13}C NMR (101 MHz, $CDCl_3$): δ, ppm 53.6, 40.3. IR; 3363 ν_{N-H} (br) , 2938 $\nu_{sp^3\,C-H}$ (w), 2097 $\nu_{N=N=N}$ (m), 1574 ν_{N-H} (w).

The 2-azidoethanamine formed was immediately reacted with rhodamine 6G (0.495 g, 0.001 mols) in methanol in a 9:1 molar ratio. The mixture refluxed overnight, yielding compound **3.4** (0.473 g, 0.001 mols, 95.0 %). ^{1}H NMR (400 MHz, $CDCl_3$): δ, ppm 7.96 - 7.93 (1H, m), 7.48 - 7.45 (2H, m), 7.07 - 7.04 (1H, m), 6.35 (2H, s), 6.23 (2H, s), 3.53 (2H, t, *J* = 5.1 Hz), 3.29 (2H, t, *J* = 7.0 Hz), 3.26 - 3.18 (4H, m), 2.94 (2H, t, *J* = 7.0 Hz), 1.91 (6H, s), 1.33 (6H, t, *J* = 7.1 Hz). ^{13}C NMR (101 MHz, $CDCl_3$): δ, ppm 168.4, 153.5, 151.7, 147.6, 132.7, 130.8, 128.4, 128.2, 123.8, 123.0, 105.7, 96.5, 65.0, 48.8, 39.0, 38.4, 16.7, 14.7. IR; 3369 ν_{N-H} (w), 2969, 2928 $\nu_{sp^3\,C-H}$ (w), 2100 $\nu_{N=N=N}$ (m), 1682 $\nu_{C=O}$ (s).

3-formyl-1,2-phenylene dimethanesulfonate (3.6)

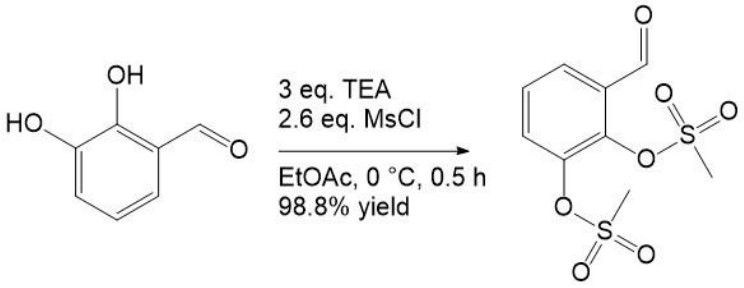

3.5 **3.6**

2,3-dihydroxybenzaldehyde (2.00 g, 0.014 mmol) was dissolved in ethyl acetate (EtOAc) in a round bottom flask (100 mL) and cooled to 0 °C by placing the flask in an ice bath. Triethylamine (TEA, ~6.0 mL, 0.044 mol) was added to the solution in the flask before mesyl chloride (2.9 mL, 0.038 mol) was added in a dropwise fashion. A yellow precipitate formed as the mesyl chloride was added. The mixture reacted for 30 minutes before quenching with water and extracting with EtOAc. The resulting organic layers were dried using magnesium sulfate ($MgSO_4$). The $MgSO_4$ was filtered out of the solution, and excess solvent was removed from the filtrate under reduced pressure to

yield compound **3.6**, a thick orange oil (4.20 g, 0.014 mols, 98.8% yield). ^{1}H NMR (400 MHz, $CDCl_3$): δ, ppm 10.23 (1H, s), 7.89 (1H, dd, *J* = 1.5, 7.9 Hz), 7.73 (1H, dd, *J* = 1.6, 8.2 Hz), 7.52 (1H, t, *J* = 8.0 Hz), 3.44 (3H, s), 3.30 (3H, s). ^{13}C NMR (101 MHz, $CDCl_3$): δ, ppm 142.3, 141.9, 131.7, 129.2, 128.9, 128.5, 39.7, 38.8. IR; 3030 $\nu_{sp^2\ C\text{-}H}$ (w), 2929, 2894 $\nu_{sp^3\ C\text{-}H}$ (w), 1699 $\nu_{C=O}$ (s).

3-(hydroxymethyl)-1,2-phenylene dimethanesulfonate (3.7)

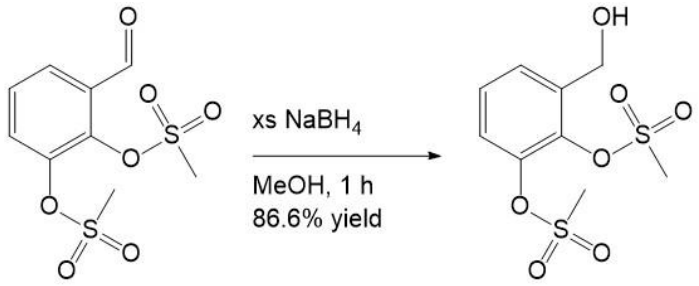

3.6 **3.7**

The reduction of the aldehyde was modified from the literature.[53] 3-formyl-1,2-phenylene dimethanesulfonate (2.00 g, 0.007 mol) and methanol (~3 mL) were combined in a round bottom flask. A stir bar was added to the flask to stir the solution before the dropwise addition of sodium borohydride ($NaBH_4$, 0.515 g, 0.014 mol) in methanol over 10 minutes. The mixture stirred for 30 minutes as the originally dark orange solution turned pale yellow with the addition of $NaBH_4$. Methanol was evaporated from the mixture before extracting the remaining sample with EtOAc and water. The resulting organic layer was dried using Na_2SO_4. The dried organic layers were filtered using celite, and excess solvent was removed from the filtrate under reduced pressure to yield compound **3.7**, a thick pale-yellow oil (1.74 g, 0.006 mols, 86.6% yield). ^{1}H NMR (400 MHz, $CDCl_3$): δ, ppm 7.49 (1H, dd, *J* = 2.1, 7.4 Hz), 7.39 (2H, dd, *J* = 2.0, 8.2 Hz), 7.34 (2H, t, *J* = 7.8 Hz), 4.73 (2H, s), 3.38 (3H, s), 3.21 (3H, s), 2.74 (1H, s). ^{13}C NMR (101

MHz, $CDCl_3$): δ, ppm 141.7, 139.1, 137.5, 128.9, 128.4, 122.7, 59.9, 39.4, 38.4. IR; 3533 ν_{O-H} (s), 3021 $\nu_{sp^2\ C-H}$ (w), 2936 $\nu_{sp^3\ C-H}$ (w).

3-(bromomethyl)-1,2-phenylene dimethanesulfonate (3.8)

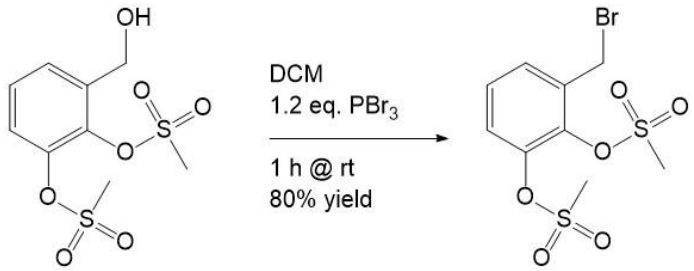

3.7 **3.8**

3-(hydroxymethyl)-1,2-phenylene dimethanesulfonate (1.66 g, 0.006 mol) and dichloromethane (DCM, ~10 mL) were added to a round bottom flask and cooled to 0 °C by placing the flask in an ice bath. A micropipette was used to add phosphorous tribromide (PBr_3, 0.639 mL, 0.007 mol) to the flask before the mixture reacted for 1 h at room temperature. After 1 h, the mixture in the flask was extracted with DCM and water. The resulting organic layers were washed with brine and dried using $MgSO_4$. The $MgSO_4$ was filtered out of the solution, and excess solvent was removed from the filtrate under reduced pressure to yield compound **3.8**, a beige solid (1.60 g, 0.005 mols, 80.0% yield). ^{1}H NMR (400 MHz, $CDCl_3$): δ, ppm 7.49 (1H, dd, *J* = 1.7, 3.7 Hz), 7.46 (1H, dd, *J* = 1.6, 4.5 Hz), 7.35 (1H, dd, *J* = 7.7, 8.4 Hz), 4.60 (2H, s), 3.46 (3H, s), 3.24 (3H, s). ^{13}C NMR (101 MHz, $CDCl_3$): δ, ppm 142.0, 139.4, 134.5, 130.2, 128.4, 123.5, 39.9, 38.4, 26.3. IR; 3084, 3032 $\nu_{sp^2\ C-H}$ (w), 2934 $\nu_{sp^3\ C-H}$ (w), 1586 $\nu_{C=C}$ (w).

Mesyl protected tripodal arm (3.9)

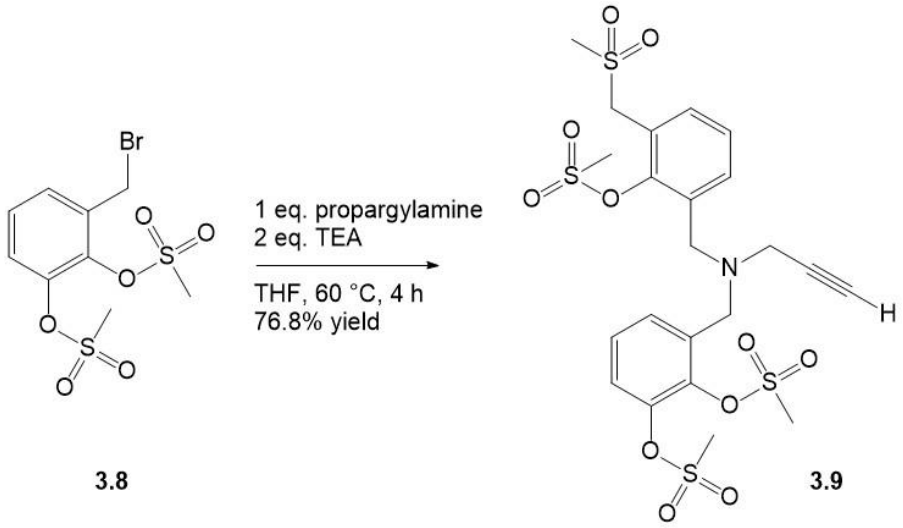

3-(bromomethyl)-1,2-phenylene dimethanesulfonate (0.50 g, 0.001 mol), tetrahydrofuran (THF, ~4 mL), TEA (0.390 mL, 0.003 mol), and propargylamine (0.096 mL, 0.001 mol) were added to a round bottom flask. The solution in the flask was stirred and refluxed for 4 h. Another addition of **3.8** (0.50 g, 0.001 mol), THF (~4 mL), and TEA (0.390 mL, 0.003 mol) was added to the crude product and allowed to react overnight. The resulting mixture was extracted using DCM and water before the aqueous layer was washed with brine. The washed aqueous layer was dried and filtered using $MgSO_4$ and celite, respectively, before concentrating the filtrate under reduced pressure to yield compound **3.9** (0.657 g, 0.001 mols, 76.8%). ^{1}H NMR (400 MHz, $CDCl_3$): δ, ppm 7.57 (1H, dd, *J* = 1.6, 7.8 Hz), 7.50 (1H, dd, *J* = 1.6, 7.7 Hz), 7.42 (1H, dd, *J* = 1.7, 5.2 Hz), 7.40 (1H, dd, *J* = 1.8, 5.3 Hz), 7.33 (2H, dt, *J* = 2.4, 11.9 Hz), 4.01 (2H, s), 3.90 (2H, s), 3.46 (2H, d, *J* = 2.4 Hz), 3.44 (3H, s), 3.35 (3H, s), 3.24 (3H, s), 3.22 (3H, s), 2.27 (1H, t, *J* = 2.4 Hz). ^{13}C NMR (101 MHz, $CDCl_3$): δ, ppm 141.9, 140.2, 135.1, 129.7, 127.9, 122.2, 51.9, 42.3, 39.7, 38.3. IR; 3283 $\nu_{sp\ C\text{-}H}$ (w), 3033 $\nu_{sp^2\ C\text{-}H}$ (w), 2921, 2850 $\nu_{sp^3\ C\text{-}H}$ (w), 1584 $\nu_{C=C}$ (w).

Attempted preparation of tripodal sensor (3.10)

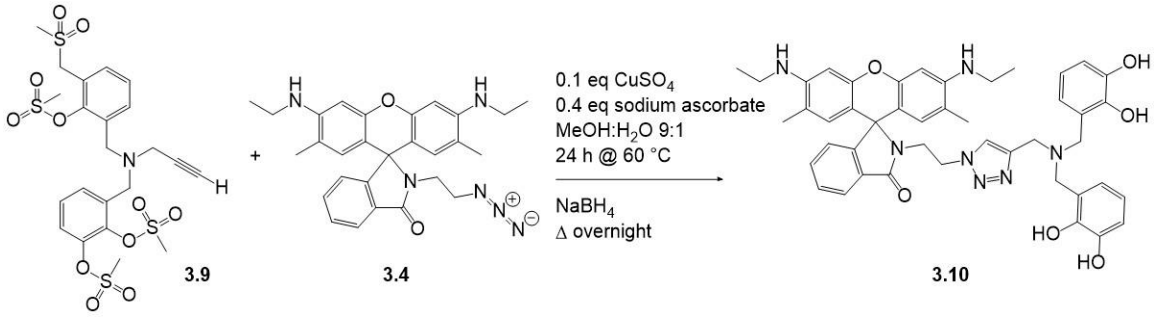

The attempted preparation of compound **3.10** involves dissolving compound **3.9** (1 eq) and rhodamine 6G azide (1 eq) in a methanol and water solution. Copper(II) sulfate ($CuSO_4$, 0.1 eq) and sodium ascorbate (0.4 eq) would be added to the solution before stirring at 60 °C for 24 h. A deprotection would then be attempted by reacting the extracted product with $NaBH_4$ overnight to yield sensor **3.10**.

Chapter 4 – Results and Discussion

4.1 Synthesis of the Rhodamine Portion of the Sensor

With the exception of the final click step in the synthesis of the sensor, each intermediate compound was successfully completed, isolated and characterized. The synthesis of the tripodal molecular sensor **3.10** was carried out via a multistep approach beginning with the synthesis of rhodamine 6G azide in a two-step one-pot synthesis (Scheme 4.1). 2-Bromoethylamine reacted with sodium azide to form compound **3.2**. The resulting azide group can readily be detected through IR analysis as the azide exhibits a strong characteristic stretch near 2100 cm^{-1}. The appearance of the azide stretch would indicate the successful formation of compound **3.2**. Compound **3.2** is extremely volatile; therefore, the reaction was carried out in situ in a one-pot reaction synthesis as rhodamine 6G in methanol was added to the mixture at the completion of the first reaction. The reaction of the azide with the rhodamine formed compound **3.4** with the spirolactam ring characteristic of "off-on" rhodamine-based sensors. The synthesis of the rhodamine 6G azide is vital to the coordination mechanism of the final tripodal sensor as one of the nitrogen atoms from the azide would act as a Lewis base to coordinate Fe^{3+} ions present.

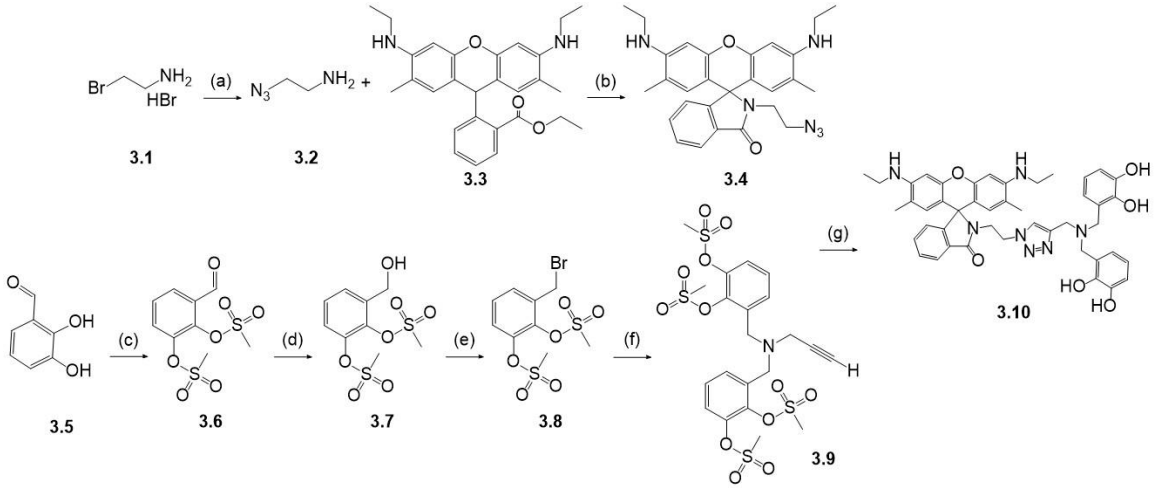

*Scheme 4.1: Complete synthesis of tripodal molecular sensor **3.10**. (a) NaN_3, water, 75 °C for 24 hrs, KOH; (b) MeOH, reflux overnight; (c) 3 eq. TEA, 2.6 eq. MsCl, EtOAc, 0 °C for 0.5 hrs; (d) xs $NaBH_4$,*

MeOH, 1 hr; (e) DCM, 1.2 eq. PBr_3, rt for 1 hr; (f) 1 eq. propargylamine, 2 eq. TEA, THF, 60 °C for 4 hrs; (g) 0.1 eq. $CuSO_4$, 0.4 eq. sodium ascorbate; MeOH:H_2O 9:1, 60 °C for 24 hrs, $NaBH_4$ Δ overnight.

4.2 Addition of Catechol Groups to Emulate Natural Siderophores

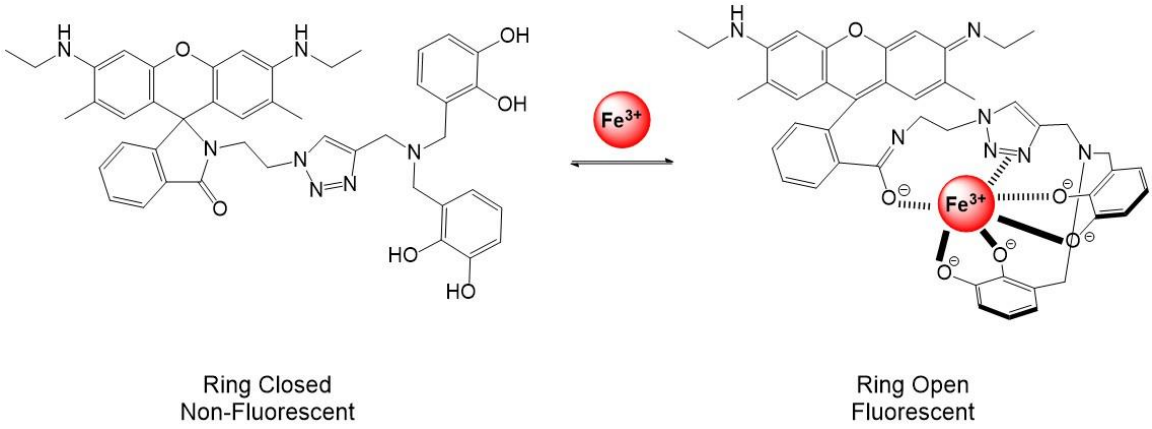

*Scheme 4.2: Proposed mechanism of coordination for the attempted sensor **3.10**.*

The overall synthetic approach was the attempted preparation of a molecular probe that behaves as an artificial siderophore. The target molecule **3.10** is a tripodal molecular probe that will bind ferric ions within the cavity (Scheme 4.2). This binding motif was chosen as we anticipate that coordination environment would increase the binding constant of Fe^{3+} ions. Thus, the motifs incorporated into the organic scaffold were chosen to enhance coordination by mimicking the structure of a natural siderophore, such as Enterobactin, a known iron chelator (Figure 4).

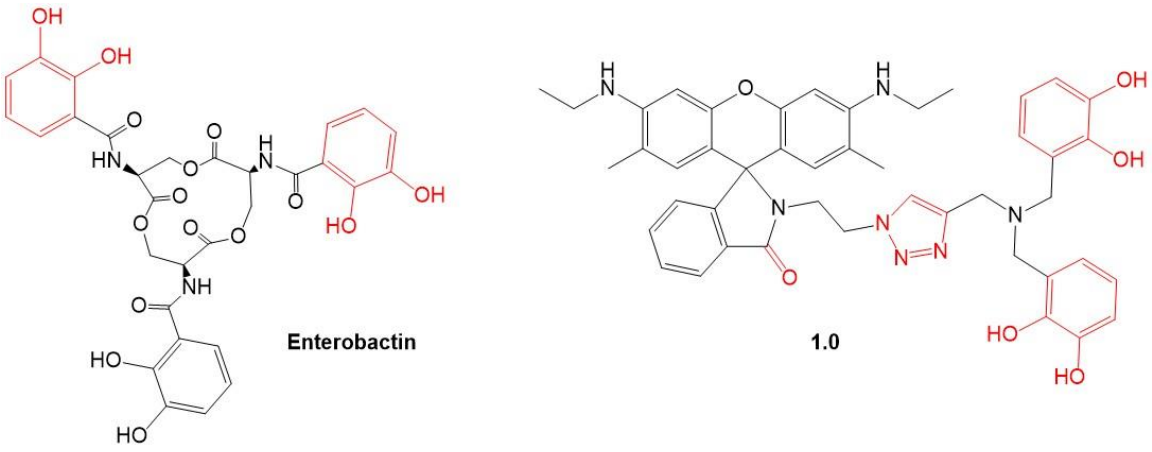

Figure 4: Comparison between characteristic catechol groups on Enterobactin and the synthesized sensor.

The tripodal arm portion of sensor **3.10** was synthesized from a four-step process involving the protection of the catechol groups of the starting material **3.5**. 2,3-dihydroxybenzaldehyde, TEA, and mesyl chloride were reacted to yield compound **3.6** with mesyl-protected catechol groups. The success of this protection step could be monitored using IR analysis. The starting material **3.5** would have broad peaks near 3200 cm^{-1} to indicate the presence of catechol groups. If the reaction proved to be successful, the broad alcohol (OH) peaks would disappear, and peaks for the added carbonyls in the mesyl groups on compound **3.6** would appear near 1400 cm^{-1}.[54] Initially, the catechol groups were protected using methyl groups. These protecting groups proved difficult to remove in the final workup. A boron tribromide deprotection was performed but resulted in low yields and difficult-to-separate byproducts, including methylbromide and hydrobromic acid. A deprotection using aluminum trichloride was also unsuccessful in removing the protecting group without forming unfavorable byproducts. Tert-butyldimethylsilyl chloride (TBDMS) as a protecting group was a successful alternative approach to the initial procedures. However, the mesyl protecting groups ultimately used for protecting the catechol groups increased the efficiency of the protection and deprotection steps and was chosen over TBDMS.

After the protection step, the aldehyde functional group on compound **3.6** was reduced to a primary OH using $NaBH_4$, a common reducing agent. ^1H NMR would show the success of the reduction when the aldehyde signal at 10.23 ppm disappeared, and a new signal near 4-5 ppm appeared, signifying the reduction of the sp^2 hybridized carbon to a sp^3 hybridization. Similar to the IR analysis for compound **3.6**, the appearance of a broad OH peak near 3200 cm^{-1} while retaining the carbonyl peaks from the mesyl groups

would suggest the reaction was successful in reducing the aldehyde to a primary OH and yielding compound **3.7**. Compound **3.7** was reacted with PBr_3 to promote a nucleophilic substitution of the OH with bromine and to form compound **3.8**. The progress of this reaction analyzed using IR would indicate success when the broad OH peak disappeared. The stretching for the halide on compound **3.8** would appear in the fingerprint region (700-500 cm^{-1}) of the IR spectra.[55]

Compound **3.8** and propargylamine were reacted to synthesize the mesyl protected tripodal arm portion, compound **3.9**, of the final sensor. The experimental procedures performed to synthesize compound **3.9** yielded two products: compound **3.9** with two additions of **3.8** and a product with one addition of **3.8**. The other product occurred when the nucleophilic substitution mechanism failed to occur twice to produce the desired compound **3.9**. The successful synthesis of compound **3.9** in the mixture could be determined by MS analysis (*m/z* = 612.1). An MS analysis of the mixture would separate both products by mass and allow for the determination of the formation of compound **3.9**. The other product with only one addition of compound **3.8** would appear in a mass spectrum with *m/z* = 334.2; whereas, compound **3.9** would exhibit a *m/z* = 612.1. Other methods including NMR and IR would prove the product challenging to separate, resulting from the symmetry of compound **3.9** and similarities in functional groups of both products, respectively.

The mixture of major and minor products from the tripodal arm reaction would be used to attempt the final sensor **3.10** synthesis. The products of the previous reaction, $CuSO_4$, and sodium ascorbate would be reacted to yield the mesyl protected sensor. A deprotection using $NaBH_4$ would be carried out overnight to yield the final tripodal

sensor **3.10** with deprotected catechol groups. The products should produce sensor **3.10**, and another product resulting from the click reaction between the other tripodal arm product and rhodamine 6G azide. The final sensor required two catechol groups to better mimic the structure of Enterobactin's three catechol group design (Figure 4). The success of the click reaction could be verified using MS analysis as the desired mesyl protected sensor would exhibit a *m/z* = 1094.3. Additionally, IR analysis would indicate successful deprotection as broad OH peaks near 3200 cm^{-1} should appear.

Chapter 5 – Conclusion

The purpose of this research was to synthesize a rhodamine-based artificial siderophore with improved selectivity for Fe^{3+}. Although rhodamine-based probes in the literature proved to be sensitive to Fe^{3+} ions, interference from other metal ions continued to appear regardless of the claimed "selectivity." To improve Fe^{3+} selectivity, the synthesis of a tripodal molecular sensor was attempted through the proposed mechanism (Scheme 4.1). Rhodamine 6G azide was successfully synthesized from rhodamine 6G and 2-azidoethanamine. Additionally, the tripodal arm portion of the sensor was successfully formed. The research covered in this thesis did not advance to form the final sensor or perform the deprotection of the catechol groups. In future research, the rhodamine 6G azide and tripodal arm will undergo a click reaction to yield the final sensor. The deprotection of the alcohols will then be performed to yield the catechol motifs expected to coordinate with Fe^{3+} ions. Further studies to be performed will assess the sensor's complexation properties, binding constants, and spectroscopic characterization to further ascertain the sensor's selective binding capabilities to Fe^{3+} ions.

References

(1) Lin, Y.-L.; Sung, R.; Sung, K. Bis(Rhodamine)-Based Polyether Type of Turn-on Fluorescent Sensors: Selectively Sensing Fe(III). *Tetrahedron* **2016**, *72*, 5744–5748.

(2) Lin, F.; Cai, J.; Li, Y.; Yu, H.; Li, S. Constituting Fully Integrated Colorimetric Analysis System for Fe(III) on Multifunctional Nitrogen-Doped MoO3/Cellulose Paper. *Talanta* **2018**, *180*, 352–357.

(3) Nielsen, F. H. Trace Elements. *Encyclopedia of Food Sciences and Nutrition*; Academic Press, 2003; pp 5820–5828.

(4) Shapiro, J. A.; Wencewicz, T. A. Acinetobactin Isomerization Enables Adaptive Iron Acquisition in Acinetobacter Baumannii through PH-Triggered Siderophore Swapping. *ACS Infect. Dis.* **2016**, *2*, 157–168.

(5) Hocking, R. K.; DeBeer George, S.; Raymond, K. N.; Hodgson, K. O.; Hedman, B.; Solomon, E. I. Fe L-Edge X-Ray Absorption Spectroscopy Determination of Differential Orbital Covalency of Siderophore Model Compounds: Electronic Structure Contributions to High Stability Constants. *J. Am. Chem. Soc.* **2010**, *132*, 4006–4015.

(6) Meneely, K. M.; Ronnebaum, T. A.; Riley, A. P.; Prisinzano, T. E.; Lamb, A. L. Holo Structure and Steady State Kinetics of the Thiazolinyl Imine Reductases for Siderophore Biosynthesis. *Biochemistry* **2016**, *55*, 5423–5433.

(7) Su, Q.; Guan, T.; He, Y.; Lv, H. Siderophore Biosynthesis Governs the Virulence of Uropathogenic Escherichia Coli by Coordinately Modulating the Differential Metabolism. *J. Proteome Res.* **2016**, *15*, 1323–1332.

(8) Inomata, T.; Eguchi, H.; Funahashi, Y.; Ozawa, T.; Masuda, H. Adsorption Behavior of Microbes on a QCM Chip Modified with an Artificial Siderophore–Fe3+ Complex. *Langmuir* **2012**, *28*, 1611–1617.

(9) Patel, P.; Song, L.; Challis, G. L. Distinct Extracytoplasmic Siderophore Binding Proteins Recognize Ferrioxamines and Ferricoelichelin in Streptomyces Coelicolor A3(2). *Biochemistry* **2010**, *49*, 8033–8042.

(10) Pearson, R. G. Hard and Soft Acids and Bases. *J. Am. Chem. Soc.* **1963**, *85*, 7.

(11) Wang, K.-P.; Lei, Y.; Zhang, S.-J.; Zheng, W.-J.; Chen, J.-P.; Chen, S.; Zhang, Q.; Zhang, Y.-B.; Hu, Z.-Q. Fluorescent Probe for Fe(III) with High Selectivity and Its Application in Living Cells. *Sens. Actuators, B* **2017**, *252*, 1140–1145.

(12) Gupta, V. K.; Mergu, N.; Kumawat, L. K. A New Multifunctional Rhodamine-Derived Probe for Colorimetric Sensing of Cu(II) and Al(III) and Fluorometric Sensing of Fe(III) in Aqueous Media. *Sens. Actuators, B* **2016**, *223*, 101–113.

(13) Gai, F.; Yin, L.; Fan, M.; Li, L.; Grahn, J.; Ao, Y.; Yang, X.; Wu, X.; Liu, Y.; Huo, Q. Novel Schiff Base (DBDDP) Selective Detection of Fe (III): Dispersed in Aqueous Solution and Encapsulated in Silica Cross-Linked Micellar Nanoparticles in Living Cell. *J. Colloid Interface Sci.* **2018**, *514*, 357–363.

(14) Kilic, H.; Bozkurt, E. A Rhodamine-Based Novel Turn On Trivalent Ions Sensor. *J. Photochem. Photobiol., A* **2018**, *363*, 23–30.

(15) Piao, J.; Lv, J.; Zhou, X.; Zhao, T.; Wu, X. A Dansyl–Rhodamine Chemosensor for Fe(III) Based on off–on FRET. *Spectrochim. Acta, Part A* **2014**, *128*, 475–480.

(16) Lee, M. H.; Lee, H.; Chang, M. J.; Kim, H. S.; Kang, C.; Kim, J. S. A Fluorescent Probe for the Fe 3+ Ion Pool in Endoplasmic Reticulum in Liver Cells. *Dyes Pigm.* **2016**, *130*, 245–250.

(17) Institute of Medicine; Food and Nutrition Board. *Dietary Reference Intakes for Vitamin A, Vitamin K, Arsenic, Boron, Chromium, Copper, Iodine, Iron, Manganese, Molybdenum, Nickel, Silicon, Vanadium, and Zinc: A Report of the Panel on Micronutrients*; National Academy Press: Washington, D.C., 2001; pp 224, 290, 301.

(18) Guo, X.; Li, M.; Hou, T.; Wu, H.; Wen, Y.; Yang, H. A Novel and Stable Raman Probe for Sensing Fe (III). *Sens. Actuators, B* **2016**, *224*, 16–21.

(19) Wei, T.-B.; Yong, B.-R.; Dang, L.-R.; Zhang, Y.-M.; Yao, H.; Lin, Q. A Simple Water-Soluble Phenazine Dye for Colorimetric/ Fluorogenic Dual-Mode Detection and Removal of Cu2+ in Natural Water and Plant Samples. *Dyes Pigm.* **2019**, *171*, 107707.

(20) Wang, Y.; Mao, P.-D.; Wu, W.-N.; Mao, X.-J.; Fan, Y.-C.; Zhao, X.-L.; Xu, Z.-Q.; Xu, Z.-H. New Pyrrole-Based Single-Molecule Multianalyte Sensor for Cu2+, Zn2+, and Hg2+ and Its AIE Activity. *Sensors and Actuators B: Chemical* **2018**, *255*, 3085–3092.

(21) *Exposure to Mercury: A Major Public Health Concern*; World Health Organization: Geneva, Switzerland, 2007.

(22) Ji, C.; Miller, P. A.; Miller, M. J. Iron Transport-Mediated Drug Delivery: Practical Syntheses and In Vitro Antibacterial Studies of Tris-Catecholate Siderophore–

Aminopenicillin Conjugates Reveals Selectively Potent Antipseudomonal Activity. *J. Am. Chem. Soc.* **2012**, *134*, 9898–9901.

(23) Neff, C.; Bellot, F.; Waern, J.-B.; Lambert, F.; Brandel, J.; Serratrice, G.; Gaboriau, F.; Policar, C. Glycosiderophores: Synthesis of Tris-Hydroxamate Siderophores Based on a Galactose or Glycero Central Scaffold, Fe(III) Complexation Studies. *J. Inorg. Biochem.* **2012**, *112*, 59–67.

(24) Zane, H. K.; Butler, A. Isolation, Structure Elucidation, and Iron-Binding Properties of Lystabactins, Siderophores Isolated from a Marine Pseudoalteromonas Sp. *J. Nat. Prod.* **2013**, *76*, 648–654.

(25) Banerjee, S.; Weerasinghe, A. J.; Parker Siburt, C. J.; Kreulen, R. T.; Armstrong, S. K.; Brickman, T. J.; Lambert, L. A.; Crumbliss, A. L. Bordetella Pertussis FbpA Binds Both Unchelated Iron and Iron Siderophore Complexes. *Biochemistry* **2014**, *53*, 3952–3960.

(26) Antonietti, V.; Boudesocque, S.; Dupont, L.; Farvacques, N.; Cézard, C.; Da Nascimento, S.; Raimbert, J.-F.; Socrier, L.; Robin, T.-J.; Morandat, S.; et al. Synthesis, Iron(III) Complexation Properties, Molecular Dynamics Simulations and P. Aeruginosa Siderophore-like Activity of Two Pyoverdine Analogs. *Eur. J. Med. Chem.* **2017**, *137*, 338–350.

(27) Kobylarz, M. J.; Heieis, G. A.; Loutet, S. A.; Murphy, M. E. P. Iron Uptake Oxidoreductase (IruO) Uses a Flavin Adenine Dinucleotide Semiquinone Intermediate for Iron-Siderophore Reduction. *ACS Chem. Biol.* **2017**, *12*, 1778–1786.

(28) Li, K.; Feng, Q.; Niu, G.; Zhang, W.; Li, Y.; Kang, M.; Xu, K.; He, J.; Hou, H.; Tang, B. Z. Benzothiazole-Based AIEgen with Tunable Excited-State Intramolecular Proton Transfer and Restricted Intramolecular Rotation Processes for Highly Sensitive Physiological PH Sensing. *ACS Sens.* **2018**, *3* (5), 920–928.

(29) Wang, Y.; Song, F.; Zhu, J.; Zhang, Y.; Du, L.; Kan, C. Highly Selective Fluorescent Probe Based on a Rhodamine B and Furan-2-Carbonyl Chloride Conjugate for Detection of Fe3+ in Cells. *Tetrahedron Lett.* **2018**, *59*, 3756–3762.

(30) Senthil Murugan, A.; Vidhyalakshmi, N.; Ramesh, U.; Annaraj, J. In Vivo Bio-Imaging Studies of Highly Selective, Sensitive Rhodamine Based Fluorescent Chemosensor for the Detection of Cu2+/Fe3+ Ions. *Sens. Actuators, B* **2018**, *274*, 22–29.

(31) Luo, A.; Wang, H.; Wang, Y.; Huang, Q.; Zhang, Q. A Novel Colorimetric and Turn-on Fluorescent Chemosensor for Iron(III) Ion Detection and Its Application to Cellular Imaging. *Spectrochim. Acta, Part A* **2016**, *168*, 37–44.

(32) Liu, X.-J.; Zhang, M.; Yang, M.-P.; Li, B.; Cheng, Z.; Yang, B.-Q. Low Cytotoxicity Rhodamine-Based Fluorescent Probes for Fe(III) and Their Application in Living Cells. *Tetrahedron* **2015**, *71*, 8194–8199.

(33) Clevenger, K. D.; Wu, R.; Er, J. A. V.; Liu, D.; Fast, W. Rational Design of a Transition State Analogue with Picomolar Affinity for Pseudomonas Aeruginosa PvdQ, a Siderophore Biosynthetic Enzyme. *ACS Chem. Biol.* **2013**, *8*, 2192–2200.

(34) Wurst, J. M.; Drake, E. J.; Theriault, J. R.; Jewett, I. T.; VerPlank, L.; Perez, J. R.; Dandapani, S.; Palmer, M.; Moskowitz, S. M.; Schreiber, S. L.; et al. Identification

of Inhibitors of PvdQ, an Enzyme Involved in the Synthesis of the Siderophore Pyoverdine. *ACS Chem. Biol.* **2014**, *9*, 1536–1544.

(35) Yang, X.-H.; Li, S.; Tang, Z.-S.; Yu, X.-D.; Huang, T.; Gao, Y. A Simple, Water-Soluble, Fe3+-Selective Fluorescent Probe and Its Application in Bioimaging. *Chin. Chem. Lett.* **2015**, *26*, 129–132.

(36) Nayab, P. S.; Shkir, M.; Gull, P.; AlFaify, S. A Highly Sensitive "Off-On" Optical and Fluorescent Chemodosimeter for Detecting Iron (III) and Its Application in Practical Samples: An Investigation of Fe 3+ Induced Oxidation by Mass Spectrometry. *J. Photochem. Photobiol., A* **2017**, *347*, 209–217.

(37) Kim, H.; Rao, B. A.; Jeong, J.; Angupillai, S.; Choi, J. S.; Nam, J.-O.; Lee, C.-S.; Son, Y.-A. A Rhodamine Scaffold Immobilized onto Mesoporous Silica as a Fluorescent Probe for the Detection of Fe (III) and Applications in Bio-Imaging and Microfluidic Chips. *Sens. Actuators, B* **2016**, *224*, 404–412.

(38) Chen, X.; Sun, W.; Bai, Y.; Zhang, F.; Zhao, J.; Ding, X. Novel Rhodamine Schiff Base Type Naked-Eye Fluorescent Probe for Sensing Fe 3+ and the Application in Cell. *Spectrochim. Acta, Part A* **2018**, *191*, 566–572.

(39) Farat, O. K.; Farat, S. A.; Tatarets, A. L.; Mazepa, A. V.; Markov, V. I. Synthesis and Spectral Properties of New Xanthene Chromophores. *J. Mol. Struct.* **2019**, *1176*, 567–575. https://doi.org/10.1016/j.molstruc.2018.09.002.

(40) Wang, L.; Ye, D.; Li, W.; Liu, Y.; Li, L.; Zhang, W.; Ni, L. Fluorescent and Colorimetric Detection of Fe(III) and Cu(II) by a Difunctional Rhodamine-Based Probe. *Spectrochim. Acta, Part A* **2017**, *183*, 291–297.

(41) Chen, H.; Bao, X.; Shu, H.; Zhou, B.; Ye, R.; Zhu, J. Synthesis and Evaluation of a Novel Rhodamine B-Based 'Off-on' Fluorescent Chemosensor for the Selective Determination of Fe 3+ Ions. *Sens. Actuators, B* **2017**, *242*, 921–931.

(42) Wang, H.; Kang, T.; Wang, X.; Feng, L. Design and Synthesis of a Novel Tripod Rhodamine Derivative for Trivalent Metal Ions Detection. *Sens. Actuators, B* **2018**, *264*, 391–397.

(43) Chen, Q.; Fang, Z. Two Sugar-Rhodamine "Turn-on" Fluorescent Probes for the Selective Detection of Fe3+. *Spectrochim. Acta, Part A* **2018**, *193*, 226–234.

(44) Sasaki, H.; Hanaoka, K.; Urano, Y.; Terai, T.; Nagano, T. Design and Synthesis of a Novel Fluorescence Probe for Zn2+ Based on the Spirolactam Ring-Opening Process of Rhodamine Derivatives. *Bioorg. Med. Chem.* **2011**, *19* (3), 1072–1078.

(45) Long, Y.; Bai, Y.-J.; Zhou, J.; Yang, B. Selective and Sensitive Off-on Probes Specific for Palladium Detection and Their Application in Biological Environments. *J. Photochem. Photobiol., A* **2017**, *332*, 422–431.

(46) Xie, P.; Zhu, Y.; Huang, X.; Gao, G.; Wei, F.; Guo, F.; Jiang, S.; Wang, C. A Novel Probe Based on Rhodamine 101 Spirolactam and 2-(2′-Hydroxy-5′-Methylphenyl)Benzothiazole Moieties for Three-in-One Detection of Paramagnetic Cu2+, Co2+ and Ni2+. *Spectrochim. Acta, Part A* **2019**, *222*, 117171.

(47) Singh, A.; Sinha, S.; Kaur, R.; Kaur, N.; Singh, N. Rhodamine Based Organic Nanoparticles for Sensing of Fe3+ with High Selectivity in Aqueous Medium: Application to Iron Supplement Analysis. *Sens. Actuators, B* **2014**, *204*, 617–621.

(48) Lee, S.; Jang, H.; Lee, J.; Jeon, S. H.; Sohn, Y.; Ra, C. S. Selective and Sensitive Morpholine-Type Rhodamine B-Based Colorimetric and Fluorescent Chemosensor for Fe(III) and Fe(II). *Sens. Actuators, B* **2017**, *248*, 646–656.

(49) Mao, J.; He, Q.; Liu, W. An Rhodamine-Based Fluorescence Probe for Iron(III) Ion Determination in Aqueous Solution. *Talanta* **2010**, *80*, 2093–2098.

(50) Zhang, Z.; Deng, C.; Zou, Y.; Chen, L. A Novel Fluorescent and Colorimetric Probe for Cascade Selective Detection of Fe(III) and Pyrophosphate Based on a Click Generated Cyclic Steroid–Rhodamine Conjugate. *J. Photochem. Photobiol., A* **2018**, *356*, 7–17.

(51) Sheng, H.; Meng, X.; Ye, W.; Feng, Y.; Sheng, H.; Wang, X.; Guo, Q. A Water-Soluble Fluorescent Probe for Fe(III): Improved Selectivity Over Cr(III). *Sens. Actuators, B* **2014**, *195*, 534–539.

(52) Zhang, G.; Liu, J.; Yang, Q.; Zhuo, R.; Jiang, X. Disulfide-Containing Brushed Polyethylenimine Derivative Synthesized by Click Chemistry for Nonviral Gene Delivery. *Bioconjugate Chem.* **2012**, *23* (6), 1290–1299.

(53) Cao, J.; Ma, C.; Zang, J.; Gao, S.; Gao, Q.; Kong, X.; Yan, Y.; Liang, X.; Ding, Q.; Zhao, C.; et al. Novel Leucine Ureido Derivatives as Aminopeptidase N Inhibitors Using Click Chemistry. *Bioorg. Med. Chem.* **2018**, *26* (12), 3145–3157.

(54) Sivets, G. G. Regio- and Stereoselective Syntheses of L-Pentose Derivatives from L-Arabinose. *Tetrahedron* **2018**, *74* (9), 920–931.

(55) Pramanick, P. K.; Hou, Z.-L.; Yao, B. Mechanistic Study on Iodine-Catalyzed Aromatic Bromination of Aryl Ethers by N -Bromosuccinimide. *Tetrahedron* **2017**, *73* (50), 7105–7114.